Climate Dynamics (2005) 24: 347–354
DOI 10.1007/s00382-004-0505-y

Anders Levermann · Alexa Griesel
Matthias Hofmann · Marisa Montoya
Stefan Rahmstorf

Dynamic sea level changes following changes in the thermohaline circulation

Received: 9 July 2004 / Accepted: 15 November 2004 / Published online: 23 February 2005

Abstract Using the coupled climate model CLIMBER-3α, we investigate changes in sea surface elevation due to a weakening of the thermohaline circulation (THC). In addition to a global sea level rise due to a warming of the deep sea, this leads to a regional dynamic sea level change which follows quasi-instantaneously any change in the ocean circulation. We show that the magnitude of this dynamic effect can locally reach up to ∼1 m, depending on the initial THC strength. In some regions the rate of change can be up to 20–25 mm/yr. The emerging patterns are discussed with respect to the oceanic circulation changes. Most prominent is a south-north gradient reflecting the changes in geostrophic surface currents. Our results suggest that an analysis of observed sea level change patterns could be useful for monitoring the THC strength.

1 Introduction

Sea level in the northern Atlantic is significantly lower compared to the northern Pacific (see Figure 1a) as a result of deep water formation in the high latitudes of the North Atlantic; this leads, e.g., to a flow through Bering Strait from the Pacific to the Arctic Ocean (Wijffels et al., 1992). Hence, any major change in North Atlantic deep water (NADW) formation can be expected to cause important sea level changes around the northern Atlantic. This is a consequence of THC changes that is often overlooked (Vellinga and Wood, 2002; Schwartz and Randall, 2003).

Paleoclimatic data indicate that strong variations of the THC have occurred in the past (see references in (Clark et al., 2002; Rahmstorf, 2002)). Model simulations suggest that global warming accompanied by an increased freshwater input into the North Atlantic could result in major changes in THC strength (Manabe and Stouffer, 1993; Stocker and Schmittner, 1997; Rahmstorf, 1999; Rahmstorf and Ganopolski, 1999; Wood et al., 1999; Schaeffer et al., 2002). Recent observations show an increase by 7% in river discharge to the Arctic Ocean (Peterson et al., 2002) between 1936 and 1999 and a significant freshening of the Atlantic Ocean during the last 40 years (Dickson et al., 2002; Curry et al., 2003). Exploring possible consequences of and indicators for thermohaline circulation (THC) changes is hence of great importance. Here, we study the sea level effects of THC changes in a series of simulations with a coupled climate model that contains an ocean circulation model with explicit calculation of sea surface elevation.

It is useful to distinguish three types of sea level changes (in addition to those resulting from tectonic processes, which we will not consider here):

1. global sea level change due to changes in the amount of water in the oceans, e.g. caused by the melting of continental ice;
2. global and regional sea level change due to changes in specific volume of sea water, caused by diabatic heating;
3. regional sea level changes (with near-zero global mean) associated with changing ocean currents and a redistribution of mass in the ocean.

A change in thermohaline ocean circulation will directly affect sea level through mechanisms (ii) and (iii) (Bryan, 1996; Gregory and Lowe, 2000; Gregory et al., 2001). Model simulations suggest that following a shutdown of NADW formation, the deep ocean would warm up on a slow diffusive time scale (millennia) as the

A. Levermann (✉) · A. Griesel · M. Hofmann · S. Rahmstorf
Potsdam Institute for Climate Impact Research,
Telegraphenberg A26, 14473 Potsdam, Germany
E-mail: anders.levermann@pik-potsdam.de

M. Montoya
Facultad de Ciencias Fisicas, Universidad Complutense
de Madrid, 28040 Madrid, Spain

supply of cold waters of polar origin to the deep ocean is reduced; this leads to a slow global sea level rise (Knutti and Stocker, 2000; Bi et al., 2001; IPCC, 2001; Seidov et al., 2001) of the order of 1 m. If NADW formation shuts down in scenarios for future global warming, this sea level rise comes in addition to the rise resulting from the warming of the surface climate.

A change in THC is also associated with a change in ocean currents and a redistribution in mass, i.e. adiabatic adjustments in the density structure of the ocean. This hardly affects the global mean sea level (since the volume of sea water is not changed, except for small differential compressibility effects in the equation of state), but it can lead to rapid regional sea level changes. The time scale of these is set by the adjustment of the internal density structure of the ocean due to internal wave processes (years to decades). The adjustment of the sea surface itself to changes in circulation and density structure occurs almost instantaneously (time scale of days) through surface gravity waves.

The sea level gradients are in equilibrium with the surface currents and winds as given by the momentum balance in the upper oceanic layer

$$\rho f v = g\partial_x(\rho\eta) - \partial_z\tau_x, \tag{1a}$$

$$\rho f u = -g\partial_y(\rho\eta) + \partial_z\tau_y, \tag{1b}$$

where η is the sea surface elevation, and ρ, f and g are the density, Coriolis parameter and gravitational constant. The stress field is (τ_x,τ_y) with the wind stress field $(\tau_{ox},-\tau_{oy})$ as its upper boundary values and $u(z)$ and $v(z)$ are the horizontal velocities in the ocean. In order to isolate and study the sea level effects of THC changes, we keep the wind stress constant throughout our experiments prescribed from NCEP/NCAR reanalysis data (Kalnay et al., 1996), despite otherwise using a fully coupled ocean-atmosphere model.

2 Model and experimental set-up

The simulations discussed here were carried out using the coupled climate model CLIMBER-3α, which contains an improved version of the oceanic general circulation model MOM 3 and thereby a non-linear explicit free surface representation. The model includes interactive atmosphere (Petoukhov et al., 2000) and sea ice modules (Fichefet and Maqueda, 1997). The wind stress in CLIMBER-3α is generally given by an interactive wind anomaly model around the NCEP-NCAR reanalysis (Kalnay et al., 1996). However, in the simulations described here we use prescribed wind stress from the NCEP-NCAR reanalysis, so that the modelled sea level changes are not due to wind stress changes. In the ocean, the resolution is 3.75°×3.75° horizontally with 24 vertical levels. For a full description of the model see (Montoya et al., 2004 (under revision)).

Figure 1 shows a comparison of altimeter data from the Topex-Poseidon satellite (NOAA, 1992–1995) of the

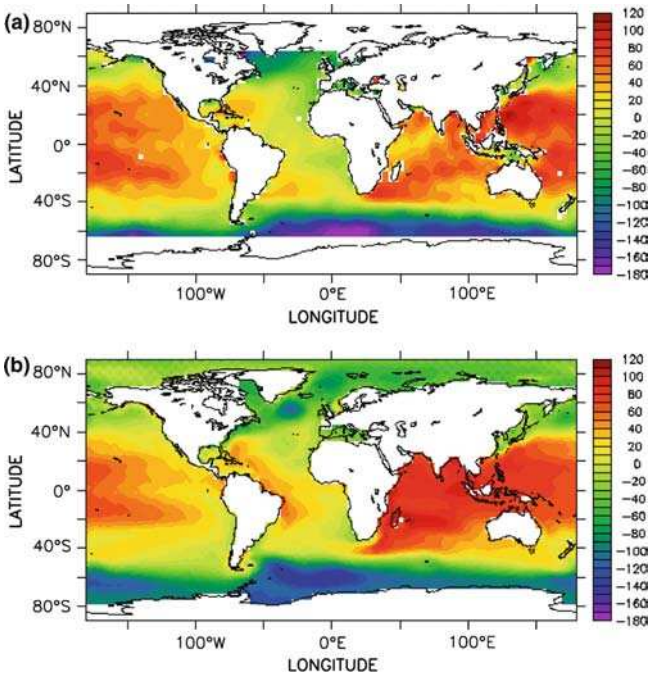

Fig. 1 Deviations of sea surface elevation from the global mean (in cm), (**a**) derived from altimeter data from the Topex-Poseidon satellite (NOAA, 1992–1995) in comparison with (**b**) a simulation of the free surface in the coupled climate model CLIMBER-3α (Montoya et al., 2004 (under revision)). Note that areas of deep convection in the northern Atlantic are associated with minima in sea level; in the altimeter data this is the Labrador Sea, while in the model it is the Irminger Sea and the Greenland-Norwegian Sea

deviation of the sea surface elevation from the geoid (normalized to give a global mean of zero), with the free surface simulation of the present-day climate with CLIMBER-3α. The model reproduces the main features of the sea level patterns. The strongest differences can be found in the Indian Ocean and along the South American East coast where too fresh surface water leads to an unrealistically high η in the model. These errors are not large, considering that this is a thermodynamic equilibrium of a coarse-resolution model without flux adjustments of heat or freshwater.

The corresponding meridional streamfunction (Figure 2a) for the same present-day equilibrium shows 12 Sv (1 Sv = 10^6 m^3 s^{-1}) overturning of NADW, a value at the lower end of observational estimates (Ganachaud and Wunsch, 2000). Figure 3 shows the mixed layer depth of the simulation. The deep water formation sites are visible as areas of deep mixed layers. NADW production takes place in the GIN Sea and Irminger Sea, while Antarctic Bottom Water is formed near the Antarctic coast in the Weddell Sea and Ross Sea. The control state simulation presented here was chosen to give the most realistic overall oceanic circulation and tracer distribution. Our results are robust with respect to changes in model parameters such as diapycnal diffusivity.

Mainly due to their thermal signature, the deep convection sites in the north can be seen as associated

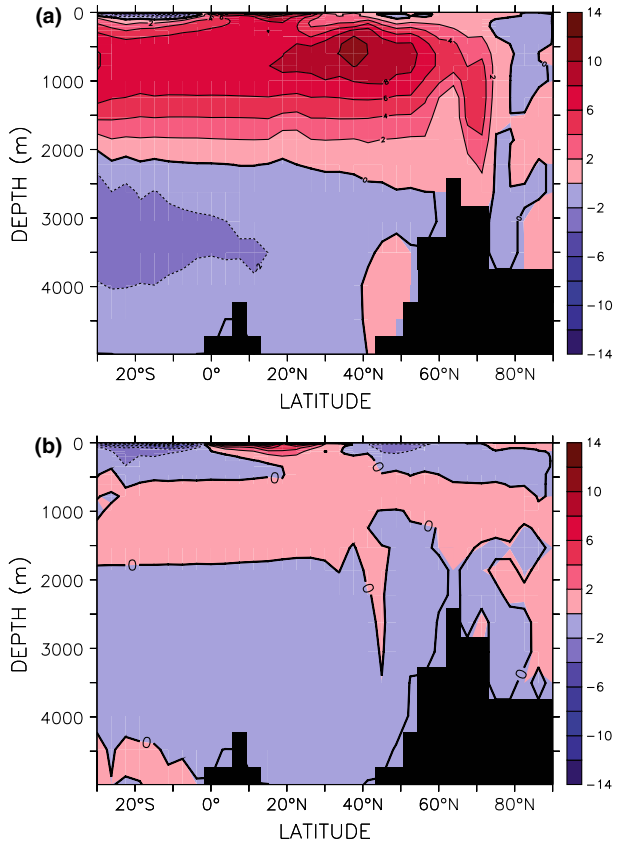

Fig. 2 Streamfunction of the meridional overturning circulation in the Atlantic Ocean (Contour line differences are 2 Sv) (**a**) for the present day equilibrium simulation (with a maximal volume transport of 12 Sv) (**b**) for an equilibrium run with an additional equivalent freshwater flux of 0.35 Sv

sea level minima in Figure 1b. The sea level difference between northern Atlantic and Pacific is 57 cm in the northernmost available strip of the altimeter data (i.e., averaged across each basin between 55°N and 65°N). In the model, this difference is underestimated as 34 cm, which is most likely due to the weak overturning; we will see later on that in the model this sea level difference is roughly proportional to the Atlantic overturning rate. Hence, our results for the sea level changes resulting from a THC shutdown should be considered as a conservative lower limit.

Starting from this present-day equilibrium state, we apply a constant negative salt flux to the two main convection sites in the North Atlantic (52°N to 80°N by 48°W to 15°E, excluding regions of shallow water along the northern European coast at 52°N to 64°N by 12°W to 8°E and along the Greenland coast at 63°N to 72°N by 31°W to 22°W), in order to cause a weakening of the overturning. A salt (rather than freshwater) flux was applied in order to avoid a sea level change due to adding water, which in the free surface formulation of our model would directly raise sea level. The THC strength decreases with increasing negative salt flux and collapses if the chosen salt flux is larger than 0.3 Sv freshwater equivalent. We used salt fluxes equivalent to 0.05, 0.075, 0.1, 0.15, 0.2, 0.25, 0.3, 0.35 and 0.4 Sv of freshwater flux which were applied until quasi-equilibrium was reached after 800 years.

Figure 2b shows the streamfunction after the application of 0.35 Sv freshwater equivalent salt flux for 800 years. In this model state, the sea level difference between northern Atlantic and Pacific is −7 cm, i.e., has almost vanished.

To check the robustness of the results, further experiments were carried out with the same oceanic model, i.e. the MOM 3 ocean model, with a slightly coarser horizontal resolution of 4°×4° coupled to the same sea ice model but with a different atmosphere model. The atmospheric module was replaced by an energy-moisture-balance model. The diapycnal diffusivity was chosen according to a Bryan-Lewis-profile with $\kappa_i = 0.6\ 10^{-4}\ m^2\ s^{-1}$in the ocean interior and $\kappa_d = 1.6\ 10^{-4}\ m^2\ s^{-1}$in the deep ocean and horizontal mixing was

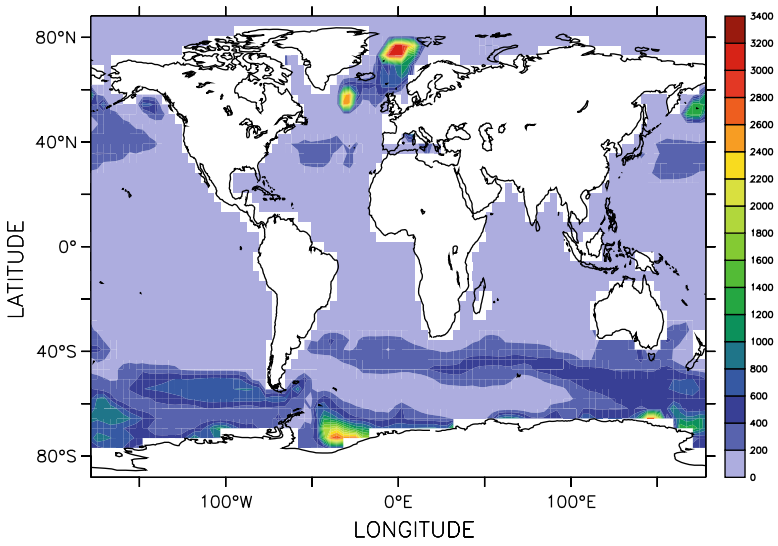

Fig. 3 Mixed layer depth (in m) for the control run. Deep water formation sites are the GIN Sea and Irminger Sea for NADW and Weddell Sea and Ross Sea for Antarctic Bottom Water

prescribed with a diffusion coefficient of $\kappa_h = 10^3$ m^2 s^{-1}. This model is bistable, showing a stable THC off-state in addition to the on-state for present-day climate (as in ref. (Manabe and Stouffer, 1988)). In this case the salt flux was removed after a brief pulse equivalent to 1 Sv for 50 years. This allowed us to examine the difference in dynamic ocean topography in the same model with the same external forcing, i.e. no additional salt flux to the northern convection sites, for a circulation with and without the THC. During the successive integration over 800 years without salt flux forcing and without THC, the sea level patterns did not change significantly. The patterns show the same structure and magnitude as the simulations shown here. We can therefore conclude that the results shown here are not due to the permanence of the salt flux applied to the Northern convection sites.

3 Time series of dynamic sea level changes associated with THC break-down

Figure 4a shows the maximum of the Atlantic overturning circulation as a function of time for a salt flux equivalent of 0.35 Sv (black line, right axis). Starting from a strength of 12 Sv, the salt flux was applied from time t = 0 onwards, causing a rapid decline of the overturning strength and its essential disappearance after 100 years. Also plotted in Figure 4a are the corresponding changes in dynamic ocean topography for different locations in the North Atlantic and the Southern Ocean (left axis). For the ten-year running average plotted in the figure, the response of the dynamic ocean topography is quasi-synchronous in the North Atlantic and in the Southern Ocean due to the fast travelling speed of the gravity waves that transport the sea level signal. Following the application of the salt flux, a positive sea level signal propagates from the North Atlantic towards the Equator (not shown). Consistent with previous theoretical work by (Hsieh and Bryan, 1996), (Johnson and Marshall, 2002) and (Johnson and Marshall, 2004) the signal takes several years to be transported across the Equator.

Sea level rise is strongest on the coasts of Europe and North America. The maximum value of 50 cm depends on the initial strength of the THC; a stronger sea level signal would result for a stronger initial overturning strength. A simulation with an increased diapycnal diffusivity of 0.4 cm^2 s^{-1} (as opposed to 0.1 cm^2 s^{-1} for the presented simulations) indeed resulted in a stronger THC of 15.5 Sv and a stronger sea level difference of 82 cm in this region. Figure 4a shows that a rapid initial sea level rise occurs within decades after the onset of the THC collapse. The rise in the North Atlantic is accompanied by a rapid decline of sea level in the Southern Ocean; the global integral of the sea level curves shown is zero, since the volume of water in the global ocean is conserved during the experiments and changes in mean specific volume (mechanism (ii) discussed in the introduction) are *not* included in this figure. The latter global

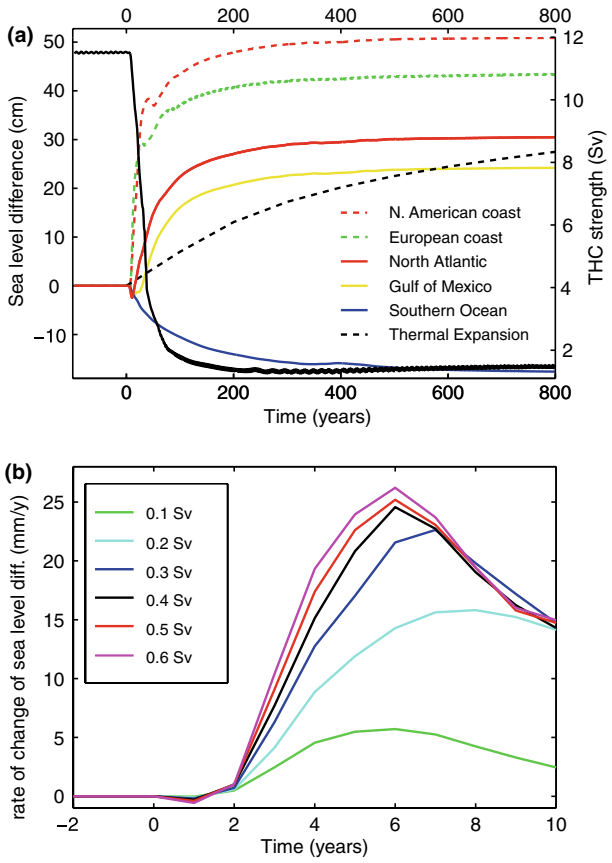

Fig. 4 (a) Time evolution (10 year running average) of the THC strength (black, right axis) and corresponding dynamic sea level changes at different locations in the North Atlantic and the Southern Ocean (left axis). Note that all regions are outside the domain of salt flux application (of 0.35 Sv). Globally averaged sea level change due to thermal expansion is shown as the black dashed line. (b) Rate of change in sea level along the North American coast for 10 year running averages and for different values of salt flux forcing. Rates of change increase for stronger weakening of the THC, but saturate after the THC collapse occurs for more than 0.3 Sv of freshwater equivalent forcing

mean change in sea level is plotted separately in Figure 4a (as a black dashed line labelled "thermal expansion"); the full sea level change is the sum of both effects (Greatbatch, 1994).

Figure 4b gives the *rate* of change of dynamic topography for the region where the Gulf Stream travels along the North American coast for different values of the salt flux applied to the northern convection sites. The rate of change varies for freshwater equivalents up to 0.3 Sv, for which the THC has weakened but not completely collapsed. For larger forcing the THC collapses and the rate of change saturates into a single curve with a maximum around 25 mm y^{-1}.

4 Patterns of dynamic sea level change

Figure 5 shows the two-dimensional pattern of the dynamic sea level change (again, the global mean of this pattern is zero). The pattern shown is the equilibrium

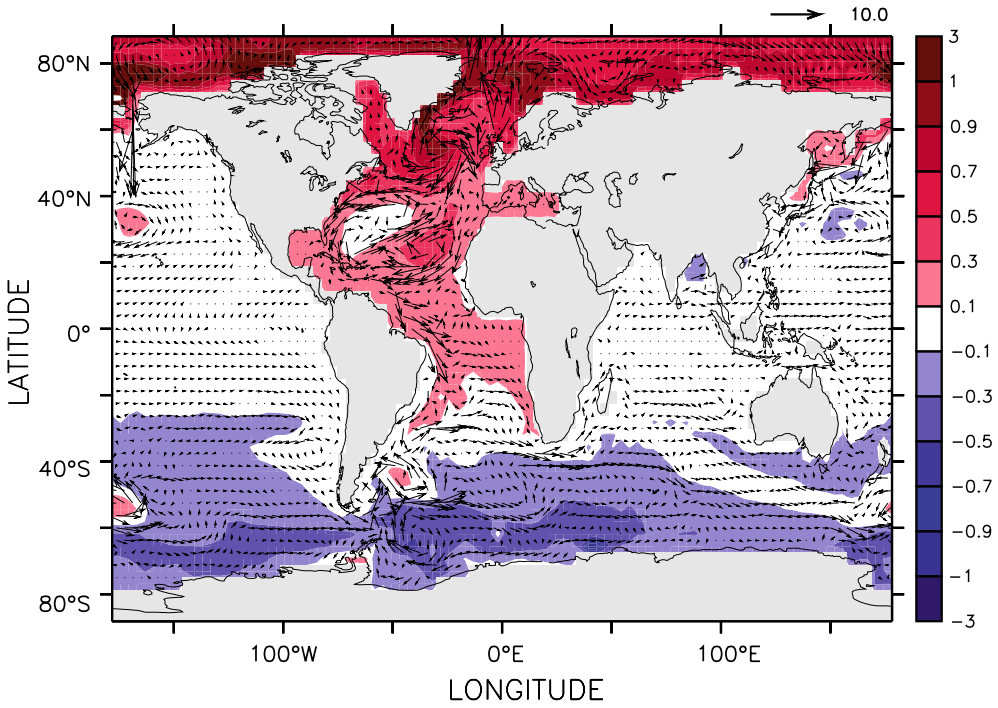

Fig. 5 Dynamic sea level changes (in m) after the collapse of the THC (colours), and difference of surface current velocities (arrow in the upper right corner corresponds to 10 cm s^{-1})

reached after the THC shutdown after 800 years integration. The sea level changes reflect the changes in the geostrophic surface currents as obtained from equations (1a,b) by omitting the wind stress terms. The ageostrophic velocities are negligible outside a strip of 3.75° (one model grid cell) around the Equator; away from the Equator the ratio of ageostrophic to geostrophic velocities is less then 1%. The wind stress was taken from the NCEP-NCAR reanalysis for all simulations, i.e. sea level differences discussed in this article are entirely due to oceanic circulation changes.

On top of the sea level differences, Figure 5 shows the difference in surface currents between the THC off-state and the THC on-state. The dominant feature in the pattern is a south-north sea level gradient, reflecting the zonal components of the upper branch of the THC. In the control run, the current crosses the Atlantic from East to West between 30°S and 40°S associated with a northward drop in sea surface elevation. The elimination of this current during a THC shutdown yields a northward sea level rise as seen in Figure 5. This effect is even clearer in the North Atlantic (around 40°N) where the Gulf Stream crosses the Atlantic basin in order to enter the GIN Sea as the North Atlantic Current. The cessation of the North Atlantic Current results in the strong northward gradient of sea level difference around 40°N and the strong onshore gradient along the North American coast seen in the figure.

The northern convection sites appear as distinct locations of sea level rise, reflecting the changes in density and the associated elimination of deep downwelling there. A strengthening of the Antarctic Circumpolar Current of about 8 Sv is seen as a sea level drop in the Southern Ocean around 60°S. Note that the formation of Antarctic Bottom Water in the present day equilibrium simulation takes place mainly through convection in the Weddell Sea and does not directly relate to the decline of sea level in the Southern Ocean.

The patterns seen in Figure 5 result from the difference in sea level between two equilibrium runs; one with and the other without additional salt flux to the northern convection sites. To confirm that the pattern obtained is robust and due to the THC change (not a direct consequence of the salt forcing), we performed a number of sensitivity experiments with varying parameter choices and with other models. When coupling the same ocean module to an energy-moisture-balance model (as described in section 2), the application of a freshwater pulse to the convection sites shuts the THC down permanently; i.e., it remains off after removal of the forcing. The sea level changes found in this off-state were of the same order of magnitude as the ones shown in Figure 5. The effect of the additional salt-flux to the northern convection sites on the sea level patterns and magnitudes in the presented simulations is negligible. The qualitative patterns and magnitudes of sea level difference shown were tested to be robust to changes in the parameter choices of the model. The simulations shown here use the parameter choice that best reproduces the present ocean circulation.

5 Sea level difference and THC strength

Figure 6 shows the sea level change for the North Atlantic coast between 45°N and 50°N and for the European coast as a function of the maximum overturning. The data plotted were obtained by equilibrium

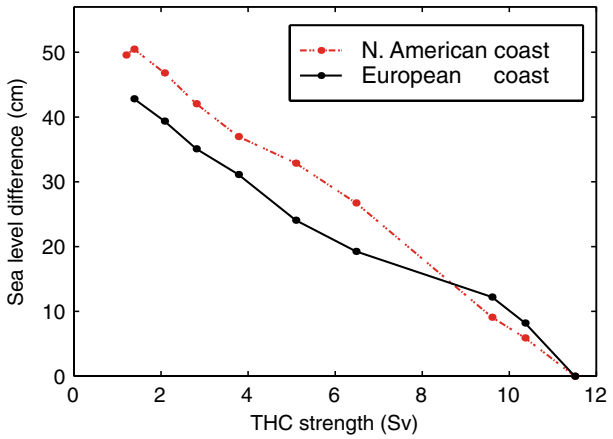

Fig. 6 Dynamic sea level changes (in cm) as a function of THC strength (in Sv) for different locations in the North Atlantic

experiments with different amounts of salt flux applied to the North Atlantic convection sites. We get a linear dependence of the sea level difference in the North American Gulf Stream region and the strength of the THC with a slope of $\gamma = 5$ cm Sv^{-1}. This slope can be understood through the geostrophic balance at the surface

$$f v_{g,\eta} = g \partial_x \eta, \tag{2}$$

where $v_{g,\eta}$ is the geostrophic surface velocity. The strength of the THC, M, can be estimated by integrating the northward velocity over a vertical box perpendicular to the North American coast.

$$M = \int_{-D}^{D} \mathrm{d}x \int_{-H}^{0} \mathrm{d}z\, v, \tag{3}$$

where the interval [-D,D] covers the zonal extension of the flow and H is its maximum depth. If, as a first approximation, we assume that the velocity v is given by $v_{g,\eta}$ for the entire box, then the integration directly yields a relation between the sea level drop and the overturning strength $\Delta\eta = \gamma \times M$. A rough estimate assuming a depth of about H = 1000 m results in a proportionality factor of $\gamma = f/(gH) = 10^{-4}$ s^{-1}/(10 m s^{-1}×1000 m) = 1 cm Sv^{-1}. In order to refine this estimate we may assume a quadratic velocity profile in the horizontal and in the vertical direction

$$M = \int_{-D}^{D} \mathrm{d}x \int_{-H}^{0} \mathrm{d}z \frac{f}{g} \partial_x \eta \frac{D^2 - x^2}{D^2} \left(\frac{H - z}{H}\right)^2 \tag{4}$$

$$\approx \frac{f}{g}\frac{\Delta\eta}{2D} \int_{-D}^{D} \mathrm{d}x \int_{-H}^{0} \mathrm{d}z \frac{D^2 - x^2}{D^2} \left(\frac{H - z}{H}\right)^2 \tag{5}$$

$$= \frac{f}{g}\frac{\Delta\eta}{2D}\frac{4D}{3}\frac{H}{3} = \frac{f}{g}\Delta\eta\frac{2}{3}\frac{1}{3} = \frac{2}{9}\frac{f}{g}\Delta\eta \tag{6}$$

where we have used the mean value theorem to get equation (5). This first order refinement yields a correction of a factor of 2/3 in the horizontal and a factor of 1/3 in the vertical directions. Thus the geostrophic slope of the red curve in Figure 6 can be estimated to be about $\gamma = 3/1 \times 3/2 \times 1$ cm Sv^{-1} = 4.5 cm Sv^{-1}, in agreement with the slope found in the model. Note, however, that this estimation is still very rough and does not take the full density distribution in the profile of the flow into account.

The scaling of sea level difference with THC strength suggests that stronger initial THC strength, compared to the rather low value of 12 Sv of our simulations, would lead to a proportionally stronger sea level response if the THC shuts down. Observations (Ganachaud and Wunsch, 2000; Talley et al., 2003) suggest higher present values for the maximum of the overturning in the Atlantic of about 16–18 Sv. Using the slope of 5 cm Sv^{-1}, this would lead to a sea level rise along the North American coast of about 80–90 cm. In order to check the effect of a stronger initial THC, we carried out simulations with increased diapycnal diffusivity. A model run with a diapycnal diffusivity of 0.4 cm^2 s^{-1} (as opposed to 0.1 cm^2 s^{-1} for the presented simulations) resulted in a stronger THC of 15.5 Sv and a sea level difference of 82 cm along the North American coast, which agrees well with the prediction from the scaling found in figure 6.

6 Implications for future climate change and THC monitoring

We have shown that a major change in THC is associated with large and potentially rapid regional sea level changes due to dynamic adjustment of the ocean surface. A complete cessation of NADW formation, for example, could raise sea level along the North American Atlantic coast by between half a meter and a meter, on a time scale that quasi-instantaneously follows the change in ocean circulation. In addition, a cessation of NADW formation would lead to a slow warming of the deep ocean, causing additional sea level rise by several decimetres, albeit on a much slower time scale. While the latter effect has been broadly discussed in the 2001 IPCC report (IPCC, 2001), the former, potentially more hazardous one has thus far received less attention (Bryan, 1996; Gregory et al., 2001).

How anthropogenic climate change will affect the ocean circulation is difficult to predict, both due to uncertainties in the freshwater budget (e.g., changes in the amount of precipitation, evaporation and Greenland melt-water runoff) and due to a strong model-dependence in the stability of the ocean circulation which is not yet understood. However, studies with coupled

atmosphere-ocean models of varying complexity (Manabe and Stouffer, 1993; Stocker and Schmittner, 1997; Manabe and Stouffer, 1999; Rahmstorf, 1999; Rahmstorf and Ganopolski, 1999; Wood et al., 1999; 2001; Stouffer and Manabe, 2003) as well as paleodata (Rahmstorf, 2002) and recent observations (Dickson et al., 2002; Peterson et al., 2002; Curry et al., 2003) suggest that a weakening or even a temporary or permanent cessation of NADW formation is within the range of possibilities.

Hence, observational monitoring of trends in the THC is important, and efforts to deploy moored arrays are in place or underway (Hirschi et al., 2003). Due to large variability and lack of long-term baseline observations, such moorings will probably only detect a change in THC when this has reached ~30% of the mean value. The specific regional pattern of sea level changes found here suggests that sea level data could be useful for monitoring changes in THC. The amplitude of 5 cm sea level rise inshore of the Gulf Stream for each Sv of weakening should be detectable. First encouraging results in this direction were presented recently (Häkkinen and Rhines, 2004) showing an increase in subpolar sea surface height during the 1990s. Häkkinen and Rhines (2004) interpreted their findings as a weakening of the THC. To which degree this reflects a long term trend or decadal variability has to be further investigated. A recent comparison of altimeter data from the Topex-Poseidon satellite between 1993 and 2003 with tide gauge measurements (Lombard et al., 2004(submitted)) is consistent with a weakening of the THC. Lombard et al. (2004) computed the residual rate of sea level rise which is not due to thermal expansion. The results show a significantly larger residual sea level rise in the North Western Atlantic (1.89 mm/yr) than in the Southern Ocean (1.11 mm/yr). Whether these regional deviations from the global mean sea level trend are due to changes in the THC strength needs to be clarified by further studies.

Acknowledgments The authors are grateful to J. Mignot for fruitful discussions. A.L. was funded by the Comer foundation. A.G. and M. H. were funded through the James S. McDonnell Foundation Centennial Fellowship. M.M. was funded by the Spanish Ministry for Science and Education through the Ramon y Cajal programme.

References

Bi D, Budd WF, Hirst AC, Wu X (2001) Collapse and reorganisation of the Southern Ocean overturning under global warming in a coupled model. Geophysical Research Letters 28(20):3927

Bryan K (1996) The steric component of sea level rise associated with enhanced greenhouse warming: a model study. Climate Dynamics 12:545

Clark PU, Pisias NG, Stocker TF, Weaver AJ (2002) The role of the thermohaline circulation in abrupt climate change. Nature 415:863

Curry R, Dickson B, Yashayaev I (2003) A change in the freshwater balance of the Atlantic Ocean over the past four decades. Nature 426:826

Dickson B, Yashayaev I, Meincke J, Turrell B, Dye S, Holfort J (2002) Rapid freshening of the deep North Altantic Ocean over the past four decades. Nature 416:832

Fichefet T, Maqueda MAM (1997) Sensitivity of a global sea ice model to the treatment of ice thermodynamics and dynamics. Journal of Geophysical Research 102:12609

Ganachaud A, Wunsch C (2000) Improved estimates of global ocean circulation, heat transport and mixing from hydrographic data. Nature 408:453

Greatbatch RJ (1994) A note on the representation of steric sea level in models that conserve volume rather than mass. Journal of Geophysical Research 99(C6):12767

Gregory JM, Lowe JA (2000) Predictions of global and regional sea-level rise using AOGCMs with and without flux adjustment. Geophysical Research Letters 27(19):3069

Gregory JM, Church JA, Boer GJ, Dixon KW, Flato GM, Jackett DR, Lowe JA, O'Farrell SP, Roeckner E, Russell GL, Stouffer RJ, Winton M (2001) Comparison of results from several AOGCMs for global and regional sea-level change 1900–2100. Climate Dynamics 18:225

Häkkinen S, Rhines PB (2004) Decline of Subpolar North Atlantic Circulation During the 1990s. Science 304:555

Hirschi J, Baehr J, Marotzke J, Stark J, Cunningham S, Beismann JO (2003) A monitoring design for the Atlantic meridional overturning circulation. Geophysical Research Letters 30(7):1413

Hsieh WW, Bryan K (1996) Redistribution of sea level rise associated with enhanced greenhouse warming: a simple model study. Climate Dynamics 12:535

IPCC (2001) Climate Change 2001: The Scientific Basis. Contribution of Working Group I to the Third Assessment Report of the Intergovernmental Panel on Climate Change. Cambridge University Press, Cambridge United Kingdom,

Johnson HL, Marshall DP (2002) A Theory for the Surface Atlantic Response to Thermohaline Variability. Journal of Physical Oceanography 32:1121

Johnson HL, Marshall DP (2004) Global Teleconnections of Meridional Overturning Circulation Anomalies. Journal of Physical Oceanography 34:1702

Kalnay E, Kanamitsu M, Kistler R, Collins W, Deaven D, Gandin L, Iredell M, Saha S, White G, Woollen J, Zhu Y, Chelliah M, Ebisuzaki W, Higgins W, Janowiak J, Mo KC, Ropelewski C, Wang J, Leetmaa A, Reynolds R, Jenne R, Joseph D (1996) The NCEP/NCAR 40-Year Reanalysis Project. Bulletin of the American Meteorological Society 77(3): 437–471

Knutti R, Stocker TF (2000) Influence of the Thermohaline Circulation on Projected Sea Level Rise. Journal of Climate 13:1997

Lombard A, Cazenave A, DoMinh K, Cabanes C, Nerem RS (2004 (submitted)): Thermosteric sea level rise for the past 50 years; comparison with tide gauges and inference on water mass contribution. Global and Planetary Change

Manabe S, Stouffer RJ (1988) Two stable equilibria of a coupled ocean-atmosphere model. Journal of Climate 1:841

Manabe S, Stouffer RJ (1993) Century-scale effects of increased atmospheric CO2 on the ocean-atmosphere system. Nature 364: 215

Manabe S, Stouffer RJ (1999) Are two modes of thermohaline circulation stable? Tellus 51A:400

Montoya M, Griesel A, Levermann A, Mignot J, Hofmann M, Ganopolski A, Rahmstorf S (2004 (under revision)): The Earth System Model of Intermediate Complexity CLIMBER-3α. Part I: description and performance for present day conditions. Climate Dynamics.

NOAA (1992–1995): Altimeter Gridded Sea Level Analysis: Sea Surface Height Anomaly, NOAA TOPEX/POSEIDON

Peterson BJ, Holmes RM, McClelland JW, Vörösmarty J, Lammers RB, Shiklomanov AI, Shiklomanov IA, Rahmstorf S (2002) Increasing River Discharge to the Arctic Ocean. Science 298:2171

Petoukhov V, Ganopolski A, Brovkin V, Claussen M, Eliseev A, Kubatzki C, Rahmstorf S (2000) CLIMBER-2: a climate

system model of intermediate complexity Part I: model description and performance for present climate. Climate Dynamics 16:1

Rahmstorf S (1999) Shifting seas in the greenhouse ? Nature 399:523

Rahmstorf S (2002) Ocean circulation and climate during the past 120,000 years. Nature 419:207

Rahmstorf S, Ganopolski A (1999) Long-term global warming scenarios computed with an efficient coupled climate model. Climatic Change 43:353

Schaeffer M, Selten FM, Opsteegh JD, Goose H (2002) Intrinsic limits to predictability of abrupt regional climate change in IPCC SRES scenarios. Geophysical Research Letters 29(16):1767

Schwartz P, Randall D (2003) An Abrupt Climate Change Scenario and Its Implications for United States National Security. Pentagon Report

Seidov D, Haupt BJ, Barron EJ, Maslin M(2001) Ocean Bi-Polar Seesaw and Climate: Southern Versus Northern Meltwater Impacts. In: The Oceans and Rapid Climate Change - Past, Present, and Future126:147

Stocker TF, Schmittner A (1997) Influence of CO2 emission rates on the stability of the thermohaline circulation. Nature 388:862

Stouffer RJ, Manabe S (2003) Equilibrium response of thermohaline circulation to large changes in atmospheric CO_2 concentration. Climate Dynamics 20:759

Talley LD, Reid JL, Robbins PE (2003) Data-Based Meridional Overturning Streamfunctions for the Global Ocean. Journal of Climate 16:3213

Vellinga M, Wood RA (2002) Global climatic impacts of a collapse of the Atlantic thermohaline circulation. Climatic Change 54:251

Wijffels SE, Schmitt RW, Bryden HL, Stigebrandt A (1992) Transport of freshwater by the oceans. Journal of Physical Oceanography 22(2):155

Wood RA, Keen AB, Mitchell JFB, Gregory JM (1999) Changing spatial structure of the thermohaline circulation in response to atmospheric CO2 forcing in a climate model. Nature 399:572